Received: 26 May 2021 | Revised: 16 July 2021 | Accepted: 16 July 2021

DOI: 10.1111/jon.12912

JOURNAL OF NEUROIMAGING
THE OFFICIAL JOURNAL OF THE AMERICAN SOCIETY OF NEUROIMAGING
WILEY

CLINICAL INVESTIGATIVE STUDY

Gray matter blood-brain barrier water exchange dynamics are reduced in progressive multiple sclerosis

Ian J Tagge[1,2] | **Valerie C Anderson**[1] | **Charles S Springer Jr.**[1] | **Manoj K Sammi**[1] | **Dennis N Bourdette**[3] | **Rebecca I Spain**[3,4] | **William D Rooney**[1,3]

[1] From theAdvanced Imaging Research Center, Oregon Health & Science University, Portland, Oregon, USA

[2] From theMontreal Neurological Institute, McGill University, Montréal, Québec, Canada

[3] From theDepartment of Neurology, Oregon Health & Science University, Portland, Oregon, USA

[4] From theNeurology Division, Veterans Affairs Portland Health Care System, Portland, Oregon, USA

Correspondence
Ian J Tagge, Montreal Neurological Institute, McGill University, 3801 Rue University, Montréal, QC H3A 2B4, Canada.
Email: ian.tagge@mcgill.ca
William Rooney, Advanced Imaging Research Center, Oregon Health & Science University, 3181 SW Sam Jackson Park Road, Portland, OR 97239, USA.
Email: rooneyw@ohsu.edu

Funding information
This research was supported by Conrad N. Hilton Foundation, NIH/NINDS (R01-NS40801, R01-EB007258, F31-NS089260), NIH/OD (S10 OD018224), NMSS (FG-1607-25259), the OHSU Brenden-Colson Center for Pancreatic Care, and the Oregon Opportunity.

Abstract

Background and Purpose: To compare transcapillary wall water exchange, a putative marker of cerebral metabolic health, in brain T_2 white matter (WM) lesions and normal appearing white and gray matter (NAWM and NAGM, respectively) in individuals with progressive multiple sclerosis (PMS) and healthy controls (HC).

Methods: Dynamic-contrast-enhanced 7T MRI data were obtained from 19 HC and 23 PMS participants. High-resolution pharmacokinetic parametric maps representing tissue microvascular and microstructural properties were created by shutter-speed (SS) paradigm modeling to obtain estimates of blood volume fraction (v_b), water molecule capillary efflux rate constant (k_{po}), and the water capillary wall permeability surface area product ($P_wS \equiv v_b{}^*k_{po}$). Linear regression models were used to investigate differences in (i) k_{po} and P_wS between groups in NAWM and NAGM, and (ii) between WM lesions and NAWM in PMS.

Results: High-resolution parametric maps were produced to visualize tissue classes and resolve individual WM lesions. Normal-appearing gray matter k_{po} and P_wS were significantly decreased in PMS compared to HC ($p \leq .01$). Twenty-one T_2 WM lesions were analyzed in 10 participants with PMS. k_{po} was significantly decreased in WM lesions compared to PMS NAWM ($p < .0001$).

Conclusions: Transcapillary water exchange is reduced in PMS NAGM compared to HC and is further reduced in PMS WM lesions, suggesting pathologically impaired brain metabolism. k_{po} provides a sensitive measure of cerebral metabolic activity and/or coupling, and can be mapped at higher spatial resolution than conventional imaging techniques assessing metabolic activity.

KEYWORDS
blood-brain barrier, cerebral metabolism, DCE-MRI, neurodegeneration, progressive multiple sclerosis

INTRODUCTION

The pathophysiological mechanisms underlying neurodegeneration in progressive forms of multiple sclerosis (PMS) are not fully understood, but a growing consensus is that chronic inflammation composed of activated microglia, macrophages, and meningeal lymphoid follicles leads to oxidative stress and mitochondrial injury.[1] Mitochondrial injury, in turn, reduces glia-neuron metabolic support, leading to additional oxidative stress, further demyelination, impaired remyelination capacity, oligodendrocyte apoptosis and axonal degeneration, and ultimately neuronal death.[2] Autopsy results show that 20%-40% of chronic lesions in PMS demonstrate ongoing inflammation and tissue destruction.[3–5] Together, these findings suggest that metabolic deficits driven by mitochondrial abnormalities may be critically important in understanding pathophysiological mechanisms associated with focal (ie, chronic active lesions) and diffuse brain tissue loss in PMS. Because standard metabolic imaging techniques (eg, PET, MR spectroscopy) suffer from poor spatial resolution,[6–8] identifying a sensitive, reliable, high spatial resolution, in vivo biomarker of brain metabolism is crucial for studying both focal and diffuse metabolic abnormalities.

Brain blood vessel properties, notably the homeostatic water molecule capillary efflux rate constant, are tightly coupled to local metabolic demands.[9] Moreover, transcapillary water exchange kinetics are amenable to mapping at high spatial resolution with shutter-speed-dynamic-contrast-enhanced MRI (SS-DCE-MRI), a two-compartment exchange model that explicitly incorporates the effects of water exchange on the MR signal.[9] With this approach, transcapillary water flux can be estimated via the trans-endothelial water exchange rate constant (k_{po}) and/or the water permeability surface area product (P_wS).[9–12] P_wS is a measure of the total water flux per unit tissue (S is the total capillary surface area per mass [or volume] of tissue), whereas k_{po} measures the kinetics of water efflux per capillary,[9] and is thus presented as a putative MRI biomarker of brain metabolism.

Here, we used low-dose gadolinium-based contrast agent (GBCA) SS-DCE-MRI to produce high-resolution parametric maps and investigate transcapillary wall water exchange kinetics in white matter (WM) lesions, normal appearing WM (NAWM), and normal appearing gray matter (NAGM) in individuals with progressive MS. We hypothesize that water flux across the capillary endothelium is driven by the activities of a large variety of transmembrane proteins, whose kinetics are rate-limited by (and thus synchronized with) those of Na^+,K^+-ATPase.[9,13,14] These, in turn, are responsive to metabolic activity behind the blood-brain barrier (BBB). We thus expect to find reduced transcapillary water exchange in PMS NAWM, NAGM, and WM lesions compared to healthy controls (HC), potentially reflecting metabolic deficits and tissue regions at risk for neurodegeneration.

METHODS

Participants

The study was approved by the local Institutional Review Board; all participants provided written informed consent. Forty-two participants (23 with clinically diagnosed primary or secondary progressive MS and 19 age- and sex-matched HC [Table 1]) were included in this study. Inclusion criteria were age 18-70 years for all subjects, and, for MS subjects, historical diagnosis of primary progressive MS based on 2010 McDonald criteria[15] or current secondary or primary progressive MS, moderate or greater neurological disability from MS with European Database for MS (EDMUS) Grading Scale[16,17] score ≥ 3.0, either taking no disease-modifying therapy or taking FDA-approved disease-modifying therapy not shown to benefit PMS. Nine PMS subjects were on disease-modifying therapy at the time of imaging (Avonex [$n = 4$], Copaxone [$n = 3$], Rebif [$n = 1$], and Tecfidera [$n = 1$]).

TABLE 1 Study population demographics

	HC ($n = 19$)	PMS ($n = 23$)
Mean age (years)	52.7 ± 11.7	57.5 ± 6.7
Age range (years)	34-70	43-65
Sex (F/M)	11/8	12[a]/11[b]
Mean disease duration (years)	–	22.9 ± 9.6
Mean EDMUS EGS	–	5.5 ± 1.2

Note: All the data represents mean ± standard deviation unless otherwise indicated.
Abbreviations: EDMUS EGS, European Database for MS Grading Scale; F, female; HC, healthy control; M, male; n, number of participants.
[a]3 Primary progressive MS (PPMS), 9 Secondary progressive (SPMS).
[b]4 PPMS, 7 SPMS.

MRI acquisition

MRI data were acquired with a Siemens MAGNETOM 7T MRI instrument (Erlangen, Germany) equipped with quadrature transmit and 24-channel phased-array receive RF coils. Anatomical imaging included 3-dimensional sagittal T_1-weighted magnetization-prepared rapid gradient-echo (MPRAGE) images (inversion time [TI]: 1050 ms; repetition time/echo time [TR/TE]: 2200/3.1 ms; flip angle [FA]: 7°; 0.7 mm isotropic resolution) and 3-dimensional sagittal T_2-weighted fluid-attenuated inversion recovery (FLAIR) images (TI/TR/TE: 2150/8000/398 ms; FA: 120°; 0.8 mm isotropic resolution). SS-DCE-MRI data were acquired with a single axial slice inversion recovery (IR) turboflash sequence (TR/TE/FA: 285 ms/1.15 ms/6°; 128 × 96 image matrix; field of view [256 × 192] mm^2; 10 mm slice thickness [40 µl nominal voxel size]; 8 TIs 147-1997 ms, 264 ms spacing) positioned in the centrum semiovale. IR-SS-DCE-MRI image sets (2.3 seconds temporal resolution, 50 image sets, 1 min 55 seconds total acquisition time) were obtained before, during, and after injection of 0.014 mmol/kg Gadoteridol (ProHance; Bracco Diagnostics, Cranbury, NJ).

Image processing and statistical analysis

R_1 (≡$1/T_1$) maps were calculated on a voxel-by-voxel basis for each IR image set in the DCE acquisition by fitting the full Bloch equation

incorporating all RF pulses and delays to the signal magnitude at each TI. Signal inversion recovery was modeled with a two-parameter single exponential, using a gradient expansion algorithm and Levenberg-Marquardt optimization. Pharmacokinetic parametric maps were created by fitting the SS-DCE-MRI data to the two-compartment Shutter-Speed Paradigm (SSP) model as described elsewhere,[9] to obtain estimates of R_{1exv} (the intrinsic extravascular ^1H_2O longitudinal relaxation rate constant [sans exchange] corrected for blood contributions), v_b (blood volume fraction), k_{po} (water molecule capillary efflux rate constant), and P_wS ($\equiv v_b{}^*k_{po}$, water capillary wall permeability surface area product).[9,12] The mathematical formulation for the SSP is given in Equation (1):[11,18]

$$R_1(t) = \frac{1}{2}\left\{\left[R_{1b}(t) + R_{1exv} + k_{po} + \frac{k_{po}p_b}{(1-p_b)}\right] - \left[\left(R_{1exv} - R_{1b}(t) - k_{po} + \frac{k_{po}p_b}{(1-p_b)}\right)^2 + \frac{4k_{po}^2 p_b}{(1-p_b)}\right]^{\frac{1}{2}}\right\} \quad (1)$$

where $R_{1exv} = \frac{R_1(0) - R_{1b}(0)p_b}{1-p_b}$, $R_{1b}(t) = R_{1b}(0) + r_1(1-h)[CA_b](t)$, *and* $p_b = v_b/f_w$.

Here, $R_1(0)$ and $R_{1b}(0)$ are pre-GBCA R_1 values of tissue and blood, and $R_1(t)$ and $R_{1b}(t)$ are the measured time-varying R_1 values in tissue and blood, respectively; r_1 is the gadoteridol relaxivity (3.3 second^{-1} mM^{-1} at 7T),[19] h is the hematocrit (approximately 0.45),[20,21] p_b is the mole fraction of tissue water in blood, f_w is the tissue volume fraction accessible to mobile aqueous solutes (approximately 0.85 in cortical GM, 0.76 in WM, and 0.82 in chronic WM lesions),[22–24] and $[CA_b]$ is the GBCA concentration in blood.[21] The venous output function, $R_{1b}(t)$, was obtained from a single voxel placed in the center of the sagittal sinus for each subject, and was temporally aligned with tissue signal to correct for delay in venous GBCA arrival.

Tissue segmentation masks were created using a bimodal Gaussian fitting of R_{1exv} histograms as previously described.[12,25] Masks were eroded and manually corrected to remove lesions and ensure at least 1 voxel gap between WM and GM masks to reduce partial volume contamination.[12] Suspected lesions identified in PMS R_{1exv} maps were confirmed by corresponding hyperintensity on T_2-weighted (T_2-w) FLAIR and hypointensity on T_1-w MPRAGE images. Lesions smaller than 2 voxels on R_{1exv} maps or adjacent to cortex were excluded to minimize partial volume contamination errors. Additionally, lesions identified on T_2-w FLAIR or T_1-w MPRAGE that were not well-represented on R_{1exv} maps (ie, smaller than 2 voxels or isointense with surrounding NAWM) were excluded to minimize partial volume contamination. Linear regression models were used to assess the association of k_{po} and P_wS in NAGM and NAWM with disease, adjusting for age and sex. A mixed effects model accounting for multiple lesions per patient was used to compare lesions to NAWM in the PMS subjects; p-values were calculated at the .05 significance level in two-tailed tests.

RESULTS

High-resolution parametric mapping with low-dose GBCA

High-resolution parametric maps representing tissue microvascular and microstructural properties were produced using one-seventh the standard clinical GBCA dose. Figure 1 displays single-voxel time course data for GM and sagittal sinus from one PMS subject in panel (A), and the corresponding SSP fit obtained from Equation (1) is shown in panel (B). Spatial resolution was sufficiently high in individual parametric maps to segment GM and WM and resolve individual WM lesions. Representative parametric maps for one HC and the same PMS subject from Figure 1 are shown in Figure 2. These maps demonstrate (i) clear GM and WM definition and contrast on all pharmacokinetic (PK) maps, and (ii) WM lesion conspicuity on R_{1exv} and k_{po} maps.

Groupwise differences in NAGM and NAWM

Average tissue SS-DCE-MRI parameters obtained from segmented NAGM and NAWM masks in HC and PMS groups are given in Table 2 and are illustrated in Figure 2 box plots. R_{1exv} is decreased in both PMS NAWM and NAGM compared to HC. v_b was not significantly different between groups in NAGM or NAWM. In NAGM, k_{po} was significantly reduced in PMS compared to HC ($p = .01$) subjects. In NAWM, k_{po} was reduced by 14% in PMS compared to HC groups, but the difference was not significant ($p = .06$). In contrast to NAWM, P_wS was significantly decreased in NAGM in PMS compared to HC ($p = .007$) groups. There was no significant effect of age, sex, or PMS subtype on any parametric estimate. Similarly, no associations were found between parametric estimates and EDMUS score or disease duration in the PMS group.

WM lesion abnormalities

Twenty-one lesions identified on R_{1exv} parametric maps corresponding to hyperintensities on T_2-w FLAIR images were found in 10 MS participants (5 male, 5 female; 1-3 lesions/subject). WM lesions were significantly different from PMS NAWM: R_{1exv} and k_{po} were significantly decreased ($p < .0001$ for both parameters), and v_b was significantly increased ($p = .036$). However, estimates varied widely across lesions, with both ranges and standard deviations exceeding those in NAGM and NAWM. None of the lesions in this analysis showed GBCA enhancement.

DISCUSSION

Chronic inflammation in MS impairs mitochondrial function and induces oxidative stress resulting in mitochondrial injury and metabolic deficiencies in both oligodendrocytes and neurons, promoting demyelination and neuronal death.[1,26,27] Detecting mitochondrial dysfunction

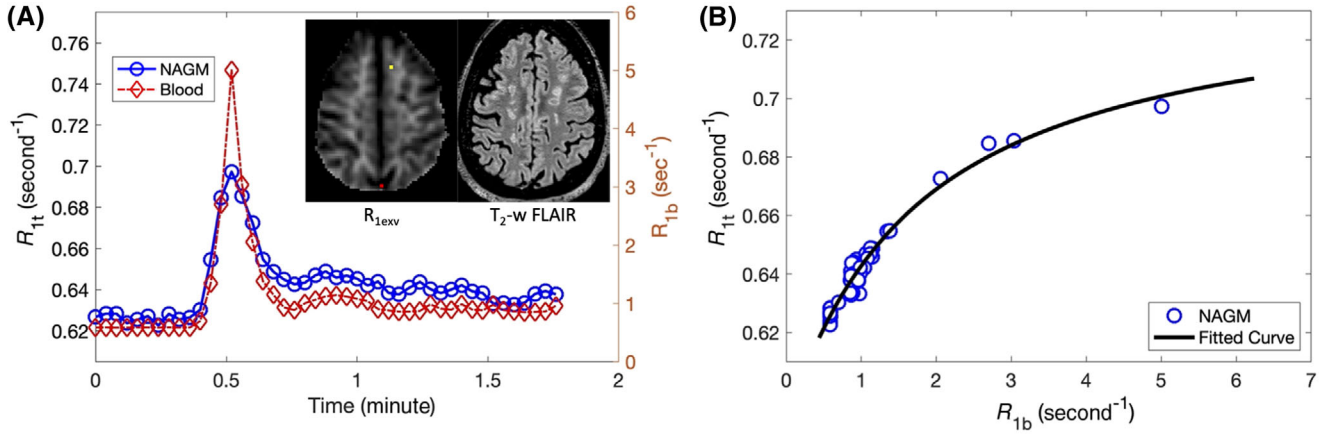

FIGURE 1 Single-voxel normal appearing gray matter (NAGM; yellow, inset) and sagittal sinus (red, inset) R_1 ($\equiv 1/T_1$) data from a 61-year-old with progressive multiple sclerosis (maps shown in Figure 2). Panel A illustrates the temporally aligned tissue (blue circles) and blood (red diamonds) response curves as a function of time during the shutter-speed dynamic-contrast-enhanced MRI acquisition (note left and right *y*-axes for tissue and blood, respectively). The corresponding R_{1b} versus R_{1t} (R_1 in tissue) plot and associated Shutter-Speed Paradigm fitted curve (solid black line) obtained from Equation (1) are shown in panel B

TABLE 2 Tissue average (± standard deviation) shutter-speed pharmacokinetic parameters

		HC	PMS	Difference	*p*-value
GM					
	R_{1exv} (s^{-1})	0.613 ± 0.036	0.562 ± 0.041	−8%	.0001
	v_b (ml/g)	0.049 ± 0.008	0.054 ± 0.012	+9%	.17
	k_{po} (s^{-1})	1.98 ± 0.42	1.64 ± 0.41	−18%	.01
	P_wS (ml/g/s)	0.095 ± 0.012	0.084 ± 0.013	−11%	.007
WM					
	R_{1exv} (s^{-1})	0.915 ± 0.023	0.857 ± 0.041	−6%	<.0001
	v_b (ml/g)	0.017 ± 0.002	0.019 ± 0.003	+9%	.06
	k_{po} (s^{-1})	3.28 ± 0.85	2.83 ± 0.70	−14%	.06
	P_wS (ml/g/s)	0.055 ± 0.011	0.052 ± 0.009	−6%	.29
WM lesions [a]					
	R_{1exv} (s^{-1})	–	0.522 ± 0.062	−39%	<.0001
	v_b (ml/g)	–	0.034 ± 0.023	+78%	.036
	k_{po} (s^{-1})	–	1.93 ± 0.71	−33%	<.0001
	P_wS (ml/g/s)	–	0.063 ± 0.038	+20%	.2

[a]Compared to normal-appearing white matter in all participants with progressive multiple sclerosis.

Abbreviations: GM, gray matter; HC, healthy control; k_{po}, water molecule capillary efflux rate constant; PMS, progressive multiple sclerosis; P_wS, water capillary wall permeability surface area product ($\equiv v_b{}^*k_{po}$); R_{1exv}, extravascular ^1H_2O relaxation rate constant; v_b, blood volume fraction; WM, white matter.

in vivo is important in understanding and monitoring subtle and potentially reversible disease activity in PMS. In this study, we find reduced transcapillary water exchange in PMS WM lesions, NAWM and NAGM, compared with healthy controls. We also find decreased R_{1exv} in both PMS NAWM and NAGM compared to HC, reflecting reduced extravascular, intracellular macromolecular content.[25,28]

Decreased transcapillary water flux could reflect a cascade of events resulting from chronic inflammation, affecting energy metabolism and ion homeostasis. The Na^+,K^+-ATPase is a ubiquitous membrane protein that is central in the establishment of ion gradients across cell membranes. Intra- and extracellular ion gradients provide the driving force for cellular work, such as substrate transport across cell membranes. After an action potential, Na^+,K^+-ATPase removes intracellular sodium in an energy-dependent process.[29] In myelinated axons, the nodes of Ranvier are enriched with Na^+,K^+-ATPase, sodium channels, and mitochondria to facilitate relatively low-energy saltatory conduction of action potentials.[30,31] However, these ion channels are redistributed after demyelination to allow the continuation of action

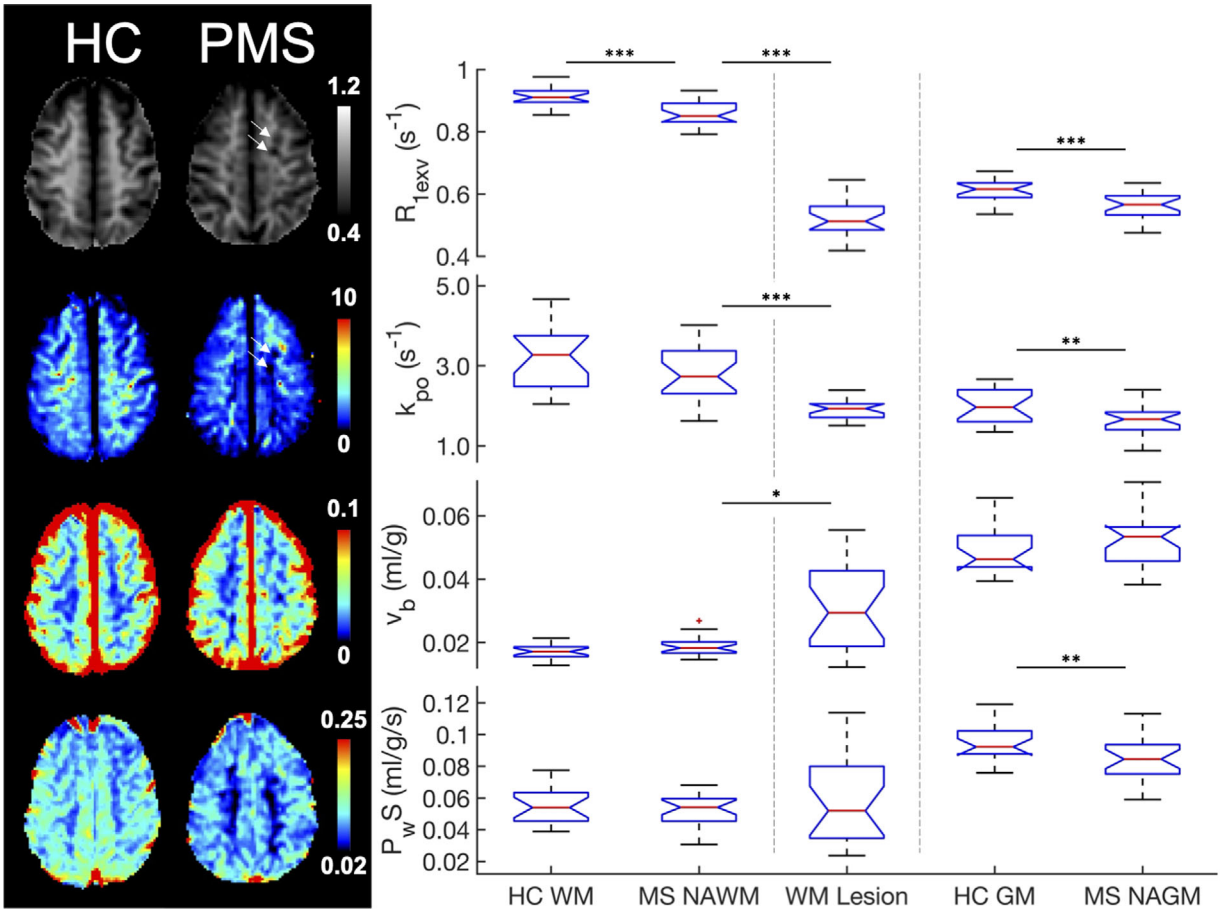

FIGURE 2 Parametric maps and group comparisons. Voxelwise parametric maps (left) from a 64-year-old healthy control (mean normal appearing white matter [NAWM] $R_{1exv} = 0.89$, $k_{po} = 3.71$, $v_b = 0.016$, $P_wS = 0.063$) and a 61-year-old with progressive multiple sclerosis (PMS, 37-year disease duration; mean NAWM $R_{1exv} = 0.81$, $k_{po} = 2.73$, $v_b = 0.017$, $P_wS = 0.048$), and corresponding group box plots (right). Color bars illustrate parametric map scales. Arrows on PMS maps highlight two hypointense WM lesions demonstrating conspicuously reduced R_{1exv} and k_{po}, suggesting permanent tissue damage (eg, potentially axonal and/or myelin loss) and a hypometabolic state, respectively. NAWM R_{1exv}, k_{po}, and P_wS are appreciably decreased in this participant with PMS. Boxplots illustrate average WM (left), WM lesions (middle), and GM (right) for all participants. Note that unscaled p_b (and $P_wS' = k_{po}{}^*p_b$) maps are shown for ease of visualization, and scaled v_b ($\equiv p_b{}^*f_w$, and $P_wS = k_{po}{}^*v_b$) values are reported for each tissue. Outliers are illustrated with "+" symbols. $^*p < .05$; $^{**}p \leq .01$; $^{***}p \leq .0001$. GM, gray matter; HC, healthy control; k_{po}, water molecule capillary efflux rate constant; p_b, mole fraction of tissue water in blood; P_wS, water capillary wall permeability surface area product ($\equiv v_b{}^*k_{po}$); R_{1exv}, extravascular ^1H_2O relaxation rate constant; v_b, blood volume fraction; WM, white matter

potentials at the cost of increased energy needs.[31–33] Mitochondria are transported to axons from neuronal cell bodies to meet the increased energy demand.[34–37] Free radical damage, potentially associated with chronic background inflammation, leads to mitochondrial and nuclear DNA mutations, mitochondrial protein degradation and lipid oxidation, and ultimately mitochondrial dysfunction.[1,31,38,39] When the compensatory axonal mitochondrial response becomes exhausted, energy demand exceeds energy supply and sodium accumulates in the axoplasm due to Na^+,K^+-ATPase dysfunction.[1,30] In addition to causing impaired nerve transmission, intracellular sodium accumulation triggers reverse Na^+/Ca^{2+} exchange,[1,36,40] which can result in calcium overload that in turn activates autolytic proteases and leads to neuronal cell death and apoptosis.[41] In addition to moving ions, membrane ion transporters also move water; it has been estimated that for each ion moved by the Na^+,K^+-ATPase, 800 water molecules also are transported.[42,43] This finding indicates that water flux across the capillary endothelium is driven by local tissue homeostatic ion pump activity, including Na^+,K^+, $2Cl^-$, and Na^+,K^+-ATPase metabolic turnover, which in turn is responsive to metabolic activity behind the BBB.[42–44] The lower the metabolic activity behind the BBB, the slower the turnover of endothelial membrane proteins associated with substrate transport and the slower the accompanying water flux. Thus, it is the tight metabolic coupling within the neurogliovascular unit that allows assessment of metabolic activity with k_{po} determined by SS-DCE-MRI at the capillary endothelial level.

A variety of multiple sclerosis neuroimaging studies have revealed diffuse abnormalities in normal appearing cortical gray matter[45] and damage can be significant even when lesion accumulation in the white matter is minimal.[46–49] Consistent with these reports, our finding of reduced k_{po} in PMS NAGM likely reflects metabolic deficits resulting

from widespread lipid oxidative injury and energy failure in cortical NAGM.[50] Because NAGM v_b is not different between groups, it is likely that P_wS differences are driven by k_{po}.

Although NAWM k_{po} differences between groups did not reach statistical significance, studies with a larger cohort and whole-brain SS-DCE-MRI may reveal significant differences in NAWM. Decreased P_wS has been reported in NAWM in a small cohort of relapsing-remitting MS ($n = 11$) subjects compared to HC ($n = 14$).[51] Slight NAWM PMS k_{po} decreases and v_b increases in PMS combine to produce P_wS values that are not different from HC at the group level in this study. This finding may reflect a pathological distinction between relapsing and progressive forms of MS but will need to be investigated further in larger cohorts. In contrast, Figure 2 parametric maps illustrate an individual with PMS in which NAWM v_b does not increase to compensate for decreased k_{po}, and thus P_wS is also reduced compared to HC in this subject.

Noncontrast MRI techniques based on diffusion-weighted (DWI) and arterial spin labeling (ASL) MRI have been used to map whole-brain P_wS and E_w (water extraction fraction, related to k_{po}) in relapsing-remitting MS.[51] Consistent with the findings in the present study, decreased P_wS was observed in chronic (non-GBCA-enhancing) MS lesions. However, all analyzed lesions were averaged together for each subject, effectively ignoring the possibility of lesion heterogeneity and masking a potentially important application of these techniques. The high degree of PK parameter variability between lesions observed in the present study may reflect lesion pathology heterogeneity (ie, a mixture of smoldering and chronic-inactive lesions), and thus may present a novel biomarker of inflammatory activity in nonenhancing WM lesions. DWI/ASL techniques have the important advantage of not requiring GBCA but are currently limited by inherently poor signal to noise ratio and thus require large (~64 µl) voxels and long acquisition times (10-20 minutes or more). Only the k_{po} factor (related to P_w) measures water "permeation"; the v_b factor (related to S) does not. Indeed, local blood volume may change in response to MS pathology or capillary dysfunction,[52–57] and thus the composite P_wS measurement may be blind to important pathological k_{po} changes.

We see the latter effect in our results (Table 2; Figure 2). Reflected as insignificant P_wS changes from HC WM to PMS NAWM to lesion, v_b changes (particularly lesion "increases") are obscuring noticeable k_{po} "decreases" (particularly in lesions). Analogous remarks can be made for the GM P_wS changes we find from HC to PMS.

We have recently used this experimental approach to report WM k_{po} decreases with HC aging.[12] Other investigators have reported BBB water permeability increases in rat brain Alzheimer's disease (AD) models.[58,59] Though the researchers used the same method as here, and measured the k_{po} and v_b factors separately, they report only the composite P_wS products. Thus, it is impossible to know if water permeation does actually increase in AD. Because the very large HC water BBB permeability[9] is metabolically controlled, it seems unlikely it would increase in pathology.

It is important to recognize that BBB permeabilities to water and GBCA differ by six orders of magnitude and do not reflect the same underlying processes, or when altered, pathologies. Increased BBB permeability to GBCA primarily reflects increased passive transcellular transport due to loss of tight junction integrity and although rate constants for these transcellular pathways increase by up to three orders of magnitude in active MS lesions compared to NAWM, in absolute terms these rate constants are still quite small compared to values for water. Although water permeability will increase through broken tight junctions, the relative increase is small because water enjoys relative high permeability across cell membranes from both passive and active processes.

The principal limitation of the present study is the limited coverage provided by the single-slice acquisition. Single-slice IR-SS-DCE-MRI was employed for this study to ensure high-fidelity pharmacokinetic modeling at the expense of limited brain coverage and increased sensitivity to motion. Through-plane motion cannot be corrected in single-slice data, and may prevent reliable parametric mapping. Alternatively, region of interest or tissue average fittings, as previously reported,[12] are less sensitive to motion artifacts and are useful in certain applications. Additionally, small lesions or those only partially contained within the centrum semiovale section used here may be included in NAWM masks. Preliminary results demonstrating feasibility of high-spatial resolution (8-20 µl voxels) 3-dimensional SS-DCE-MRI acquisitions have been presented[60,61] and will be used in future studies to overcome the limitations imposed by the single-slice acquisition in the present work.

Transcapillary water exchange may provide a window into cerebral metabolic activity and/or coupling, can be mapped at higher spatial resolution than conventional metabolic imaging techniques,[9,14] and shows promise in reflecting PMS metabolic derangements. Similarly, markedly decreased k_{po} in T_2-w lesions suggests a hypometabolic state common in chronic inactive MS lesions.[9,62] Longitudinal studies will determine if k_{po} (and/or P_wS) is sensitive to potentially hypermetabolic inflammation and microglial activation associated with chronic active lesions, and if decreased NAWM or NAGM k_{po} (and/or P_wS) is predictive of brain atrophy and clinical progression in PMS.

ACKNOWLEDGMENTS AND DISCLOSURES

The authors would like to thank Randy West and Sudeeksha Yadav for their valuable contributions to data processing and analysis.

ORCID

Ian J Tagge https://orcid.org/0000-0002-5260-7117
Valerie C Anderson https://orcid.org/0000-0001-5271-9410
Manoj K Sammi https://orcid.org/0000-0002-3556-0468
Rebecca I Spain https://orcid.org/0000-0002-8316-3723
William D Rooney https://orcid.org/0000-0003-0617-1540

REFERENCES

1. Lassmann H, van Horssen J, Mahad D. Progressive multiple sclerosis: pathology and pathogenesis. Nat Rev Neurol 2012;8:647-56.
2. Hauser SL, Chan JR, Oksenberg JR. Multiple sclerosis: prospects and promise. Ann Neurol 2013;74:317-27.
3. Lassmann H. The pathologic substrate of magnetic resonance alterations in multiple sclerosis. Neuroimaging Clin N Am 2008;18:563-76.

4. Frischer JM, Weigand SD, Guo Y, et al. Clinical and pathological insights into the dynamic nature of the white matter multiple sclerosis plaque. Ann Neurol 2015;78:710-21.
5. Sethi V, Nair G, Dewey B, et al. Slowly eroding lesions in multiple sclerosis. Neurology 2016;23:464-72.
6. Moccia M, Ciccarelli O. Molecular and metabolic imaging in multiple sclerosis. Neuroimaging Clin N Am 2017;27:343-56.
7. Swanberg KM, Landheer K, Pitt D, et al. Quantifying the metabolic signature of multiple sclerosis by in vivo proton magnetic resonance spectroscopy: current challenges and future outlook in the translation from proton signal to diagnostic biomarker. Front Neurol 2019;10:1173.
8. Bauckneht M, Capitanio S, Raffa S, et al. Molecular imaging of multiple sclerosis: from the clinical demand to novel radiotracers. EJNMMI Radiopharm Chem 2019;4:6.
9. Rooney WD, Li X, Sammi MK, et al. Mapping human brain capillary water lifetime: high-resolution metabolic neuroimaging. NMR Biomed 2015;28:607-23.
10. Springer CS, Li X, Tudorica LA, et al. Intratumor mapping of intracellular water lifetime: metabolic images of breast cancer? NMR Biomed 2014;27:760-73.
11. Li X, Rooney WD, Springer CS Jr. A unified magnetic resonance imaging pharmacokinetic theory: intravascular and extracellular contrast reagents. Magn Reson Med 2005;54:1351-9.
12. Anderson VC, Tagge IJ, Li X, et al. Observation of reduced homeostatic metabolic activity and /or coupling in white matter aging. J Neuroimaging 2020;30:658-65.
13. Zeuthen T. Water-transporting proteins. J Membr Biol 2010;234:57-73.
14. Springer CS. Using 1H2O MR to measure and map sodium pump activity in vivo. J Magn Reson 2018;291:110-26.
15. Polman CH, Reingold SC, Banwell B, et al. Diagnostic criteria for multiple sclerosis: 2010 revisions to the McDonald criteria. Ann Neurol 2011;69:292-302.
16. Confavreux C, Compston D, Hommes O, et al. EDMUS, a European database for multiple sclerosis. J Neurol Neurosurg Psychiatry 1992;55:671-6.
17. Amato MP, Grimaud J, Achiti I, et al. European validation of a standardized clinical description of multiple sclerosis. J Neurol 2004;251:1472-80.
18. Rooney WD, Yankeelov TE, Coyle PK, et al. Regional blood volumes and intravascular water lifetimes in human brain (abstract). Proc Int Soc Magn Reson Med 2003;11:2188.
19. Noebauer-Huhmann IM, Szomolanyi P, Juras V, et al. Gadolinium-based magnetic resonance contrast agents at 7 Tesla: in vitro T1 relaxivities in human blood plasma. Invest Radiol 2010;45:554-8.
20. Billett HH. Hemoglobin and hematocrit. In: Walker HK, Hall WD, Hurst JW, eds. *Clinical Methods: The History, Physical, and Laboratory Examinations*. Boston, MA: Butterworths; 1990:718-9.
21. Landis CS, Li X, Telang FW, et al. Equilibrium transcytolemmal water-exchange kinetics in skeletal muscle in vivo. Magn Reson Med 1999;42:467-78.
22. Whittall KP, MacKay AL, Graeb DA, et al. In vivo measurement of T2 distributions and water contents in normal human brain. Magn Reson Med 1997;37:34-43.
23. Laule C, Vavasour IM, Moore GRW, et al. Water content and myelin water fraction in multiple sclerosis: a T 2 relaxation study. J Neurol 2004;251:284-93.
24. Sammi MK, Silbermann E, Zarelli G, et al. Mapping temporal changes in myelin properties of newly formed Multiple Sclerosis lesions (abstract). Proc Int Soc Magn Reson Med 2020;28:0059.
25. Rooney WD, Johnson G, Li X, et al. Magnetic field and tissue dependencies of human brain longitudinal 1H2O relaxation in vivo. Magn Reson Med 2007;57:308-18.
26. Campbell GR, Worrall JT, Mahad DJ. The central role of mitochondria in axonal degeneration in multiple sclerosis. Mult Scler J 2014;20:1806-13.
27. Mahad DH, Trapp BD, Lassmann H. Pathological mechanisms in progressive multiple sclerosis. Lancet Neurol 2015;14:183-93.
28. Li X, Mangia S, Lee J, et al. NMR shutter-speed elucidates apparent population inversion of 1H2O signals due to active transmembrane water cycling. Magn Reson Med 2019;82:411-24.
29. Barnett MW, Larkman PM. The action potential. Pract Neurol 2007;7:192-7.
30. Young EA, Fowler CD, Kidd GJ, et al. Imaging correlates of decreased axonal Na+/K+ ATPase in chronic multiple sclerosis lesions. Ann Neurol 2008;63:428-35.
31. Campbell G, Mahad DJ. Mitochondrial dysfunction and axon degeneration in progressive multiple sclerosis. FEBS Lett 2018;592:1113-21.
32. Craner MJ, Hains BC, Lo AC, et al. Co-localization of sodium channel Nav1.6 and the sodium-calcium exchanger at sites of axonal injury in the spinal cord in EAE. Brain 2004;127:294-303.
33. Craner MJ, Newcombe J, Black JA, et al. Molecular changes in neurons in multiple sclerosis: altered axonal expression of Nav1.2 and Nav1.6 sodium channels and Na+/Ca2+ exchanger. Proc Natl Acad Sci 2004;101:8168-73.
34. Mahad D, Ziabreva I, Lassmann H, et al. Mitochondrial defects in acute multiple sclerosis lesions. Brain 2008;131:1722-35.
35. Witte ME, Bø L, Rodenburg RJ, et al. Enhanced number and activity of mitochondria in multiple sclerosis lesions. J Pathol 2009;219:193-204.
36. Waxman SG. Ions, energy and axonal injury: towards a molecular neurology of multiple sclerosis. Trends Mol Med 2006;12:192-5.
37. Kiryu-Seo S, Ohno N, Kidd GJ, et al. Demyelination increases axonal stationary mitochondrial size and the speed of axonal mitochondrial transport. J Neurosci 2010;30:6658-66.
38. Lassmann H. Pathology and disease mechanisms in different stages of multiple sclerosis. J Neurol Sci 2013;333:1-4.
39. Haider L, Simeonidou C, Steinberger G, et al. Multiple sclerosis deep grey matter: the relation between demyelination, neurodegeneration, inflammation and iron. J Neurol Neurosurg Psychiatry 2014;85:1386-95.
40. Stys PK, Waxman SG, Ransom BR. Ionic mechanisms of anoxic injury in mammalian CNS white matter: role of Na+ channels and Na+-Ca2+ exchanger. J Neurosci 1992;12:430-9.
41. Stys PK. General mechanisms of axonal damage and its prevention. J Neurol Sci 2005;233:3-13.
42. MacAulay N, Hamann S, Zeuthen T. Water transport in the brain: role of cotransporters. Neuroscience 2004;129:1029-42.
43. MacAulay N, Zeuthen T. Water transport between CNS compartments: contributions of aquaporins and cotransporters. Neuroscience 2010;168:941-56.
44. Lykke K, Assentoft M, Hørlyck S, et al. Evaluating the involvement of cerebral microvascular endothelial Na + /K + -ATPase and Na + -K + -2Cl – co-transporter in electrolyte fluxes in an in vitro blood–brain barrier model of dehydration. J Cereb Blood Flow Metab 2019;39:497-512.
45. Lucchinetti CF, Popescu BFG, Bunyan RF, et al. Inflammatory cortical demyelination in early multiple sclerosis. N Engl J Med 2011;365:2188-97.
46. Popescu BFG, Pirko I, Lucchinetti CF. Pathology of multiple sclerosis: where do we stand? Continuum (Minneap Minn) 2013;19:901-21.
47. De Stefano N, Matthews PM, Filippi M, et al. Evidence of early cortical atrophy in MS: relevance to white matter changes and disability. Neurology 2003;60:1157-62.
48. Calabrese M, Grossi P, Favaretto A, et al. Cortical pathology in multiple sclerosis patients with epilepsy: a 3 year longitudinal study. J Neurol Neurosurg Psychiatry 2011;83:49-54.

49. Mainero C, Benner T, Radding A, et al. In vivo imaging of cortical pathology in multiple sclerosis using ultra-high field MRI. Neurology 2009;73:941-8.
50. Haider L, Zrzavy T, Hametner S, et al. The topograpy of demyelination and neurodegeneration in the multiple sclerosis brain. Brain 2016;139:807-15.
51. Wengler K, Ha J, Syritsyna O, et al. Abnormal blood-brain barrier water exchange in chronic multiple sclerosis lesions: a preliminary study. Magn Reson Imaging 2020;70:126-33.
52. Holley JE, Newcombe J, Whatmore JL, et al. Increased blood vessel density and endothelial cell proliferation in multiple sclerosis cerebral white matter. Neurosci Lett 2010;470:65-70.
53. Girolamo F, Coppola C, Ribatti D, et al. Angiogenesis in multiple sclerosis and experimental autoimmune encephalomyelitis. Acta Neuropathol Commun 2014;2:84
54. Lengfeld J, Cutforth T, Agalliu D. The role of angiogenesis in the pathology of multiple sclerosis. Vasc Cell 2014;6:23
55. Karampoor S, Zahednasab H, Ramagopalan S, et al. Angiogenic factors are associated with multiple sclerosis. J Neuroimmunol 2016;301:88-93.
56. Angleys H, Jespersen SN, Østergaard L. The effects of capillary transit time heterogeneity (CTH) on the cerebral uptake of glucose and glucose analogs: application to FDG and comparison to oxygen uptake. Front Comput Neurosci 2016;10:1-20.
57. Østergaard L, Engedal TS, Moreton F, et al. Cerebral small vessel disease: capillary pathways to stroke and cognitive decline. J Cereb Blood Flow Metab 2016;36:302-25.
58. Dickie BR, Vandesquille M, Ulloa J, et al. Water-exchange MRI detects subtle blood-brain barrier breakdown in Alzheimer's disease rats. Neuroimage 2019;184:349-58.
59. Dickie BR, Boutin H, Parker GJM, et al. Alzheimer's disease pathology is associated with earlier alterations to blood–brain barrier water permeability compared with healthy ageing in TgF344-AD rats. NMR Biomed 2021;34:e4510.
60. Tagge IJ, Yadav S, Powers K, et al. Metabolic abnormalities associated with phase rims in progressive MS. Presented at the Americas Committee for Treatment and Research in Multiple Sclerosis 2020; February 28, 2020; Florida.
61. Tagge I, Ontaneda D, Sakaie K, et al. Leptomeningeal enhancement kinetics in relapsing-remitting MS. Presented at the Americas Committee for Treatment and Research in Multiple Sclerosis 2020; February 28, 2020; Florida.
62. Ge Y, Zhang Z, Lu H, et al. Characterizing brain oxygen metabolism in patients with multiple sclerosis with T2-relaxation-under-spin-tagging MRI. J Cereb Blood Flow Metab 2012;32:403-12.

How to cite this article: Tagge IJ, Anderson VC, Springer CS, et al. Gray matter blood-brain barrier water exchange dynamics are reduced in progressive multiple sclerosis. *J Neuroimaging*. 2021;**31:**1111–1118.
https://doi.org/10.1111/jon.12912